Energy & Buildings 331 (2025) 115379

Contents lists available at ScienceDirect

Energy & Buildings

journal homepage: www.elsevier.com/locate/enb

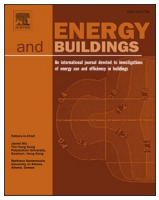

Automatic operation method using wireless sensor networks for variable refrigerant flow system: Switchless control variable refrigerant flow system

Toshihiro Suzuki [a,*], Yoshiyuki Shimoda [b], Akito Kobayashi [b], Sumio Shiochi [c]

[a] Campus Sustainability Office, Osaka University, Osaka, Japan
[b] Graduate School of Engineering, Osaka University, Osaka, Japan
[c] Technology and Innovation Center, DAIKIN INDUSTRIES, Ltd, Osaka, Japan

ARTICLE INFO

Keywords:
Variable refrigerant flow system
Energy efficiency
Medium-sized buildings
Sensor networks

ABSTRACT

Variable refrigerant flow (VRF) systems autonomously operate using built-in sensors regulated by remote settings and indoor unit intake temperatures. However, in larger spaces with multiple indoor and outdoor units, autonomous VRF systems lack the benefits of an integrated system, such as balanced load distribution, coordinated operation, and efficient ventilation. To overcome these challenges, the authors developed a "switchless VRF system" designed for small to medium-sized buildings. This system improves comfort and energy efficiency by eliminating extensive control mechanisms and switches, ensuring uniform performance and greater energy saving. We performed detailed demonstration experiments to evaluate the system's effectiveness across four key functions (pre-cooling and pre-heating, human sensing HVAC control, outdoor unit rotation control, and indoor unit fan power reduction functions). In the first control, the VRF system demonstrated significant energy efficiency, achieving 18 % energy saving in summer pre-cooling. In the second, the human-detection ventilation control effectively modulated the ventilation volume by real-time monitoring of the number of occupants, resulting in approximately 35 % energy saving. In the third, the rotational control strategy enhanced the average COP of the outdoor units by 17.7 %. In the fourth, a reduction in indoor-unit fan power led to an overall power consumption decrease of 8.6 % by ceasing fan operation when the thermostat was deactivated. This innovation addresses the modern needs of building management and energy conservation, making it a viable option for enhancing HVAC operations.

1. Introduction

The global deployment of cooling systems is on the rise, with projections indicating that the number of installed units will triple by 2050 [1]. Therefore, energy conservation in air conditioners is important to achieve carbon neutrality in the future. In particular, energy conservation in air conditioners is essential in commercial buildings, where air conditioners account for a large percentage of energy. In commercial buildings, central air conditioning systems have traditionally been the mainstream setup. In recent years, however, variable refrigerant flow (VRF) has been used worldwide, especially in Asia, owing to its simplicity of design and construction, and ease of maintenance and management. In addition, large, modern buildings with central air conditioning systems are increasingly using wireless sensor networks (WSNs) to effectively monitor the indoor environment and manage air conditioning equipment [2–5]. However, VRF systems commonly used in small and medium-sized buildings often do not have central monitoring systems such as advanced building energy management systems for cost reasons. This is partially because of the fact that VRFs are packaged equipment and that there is little information available from equipment manufacturers.

In this milieu, many researchers are still working to realize VRF systems with excellent energy performance in the operational phase, through research on advancement of elemental components of VRF [6,7], advancement of VRF systems [8,9], control methods of VRF [10,11], VRF energy performance evaluation (including comparison with other systems) [12,13], and VRF fault prediction and detection [14,15]. In the field of energy simulation, represented by EnergyPlus, research on simulation models of VRF [16,17] and analysis of VRF simulation results [18,19] are also ongoing. However, these are basic studies for further evolution of VRFs as stand-alone devices, and no study has demonstrated the effects of advanced control using external

* Corresponding author at: Campus Sustainability Office, Osaka University.
E-mail address: suzuki.toshihiro.cso@osaka-u.ac.jp (T. Suzuki).

https://doi.org/10.1016/j.enbuild.2025.115379
Received 16 October 2024; Received in revised form 23 December 2024; Accepted 24 January 2025
Available online 25 January 2025

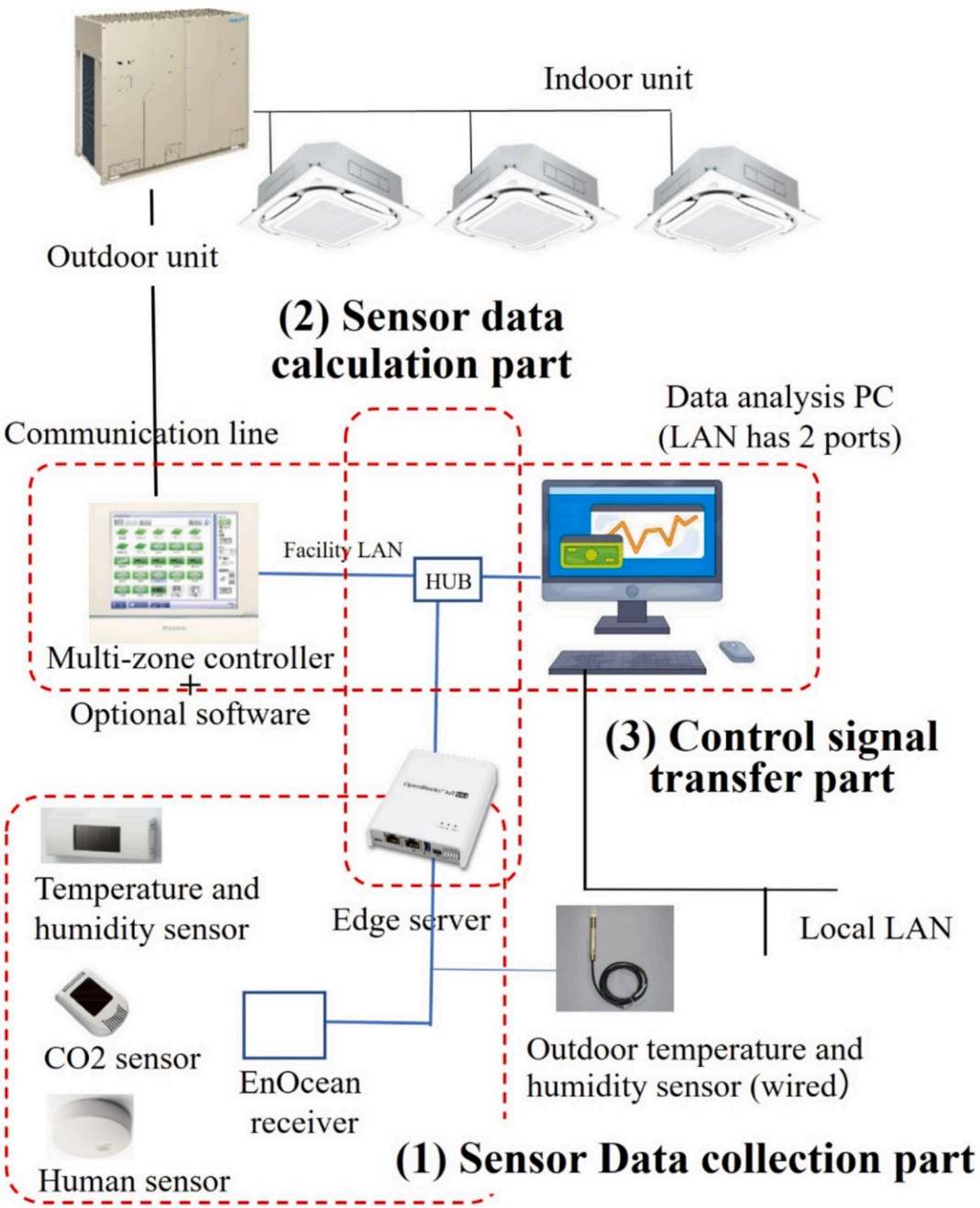

Fig. 1. System configuration.

sensors on already installed VRFs.

We believe that minimizing VRF energy loss through energy management and operating as a system through coordinated and cooperative control with ambient indoor units and ventilation systems will be important to make VRF more compatible with the carbon neutral era and achieve higher performance operation. Research on control methods that consider VRF as a system includes studies on model predictive control (MPC) of ventilation and air conditioning [20,21], which aims to achieve both thermal comfort and energy saving. Control methods have also been studied [22], including integration with humidity control devices, rather than using simple setpoint temperature control. Furthermore, a control method for determining the number of outdoor units to operate in response to load fluctuations while maintaining a uniform indoor environment during operation of a large space consisting of multiple outdoor unit systems [23] has also been studied. These studies suggest that coordinated control of VRF and other HVAC equipment, including ventilation equipment, can provide more energy-efficient operation than operating each equipment independently.

In addition, research in terms of coordination control or cooperative control of HVAC systems includes studies on air supply fan/damper operation in rooftop units (RTUs) and automatic sequence control for automatic selection of air supply fan/damper operation and operation mode (energy saving, heating/cooling, ventilation) in RTUs [24]. Research on practical model-based control for ON/OFF staging of multiple RTUs [25] and coordinated control to permanently reduce oversizing challenges in HVAC systems consisting of multiple RTUs [26] is also being conducted. However, there are no empirical studies on the latest VRFs, which are generally prevalent, especially in Asia.

The VRF system that we studied traditionally functions as a closed system facilitated by the manufacturer, with both indoor and outdoor units optimally controlled based on user settings (cooling/heating and temperature) via remote control and inlet temperature sensors on the

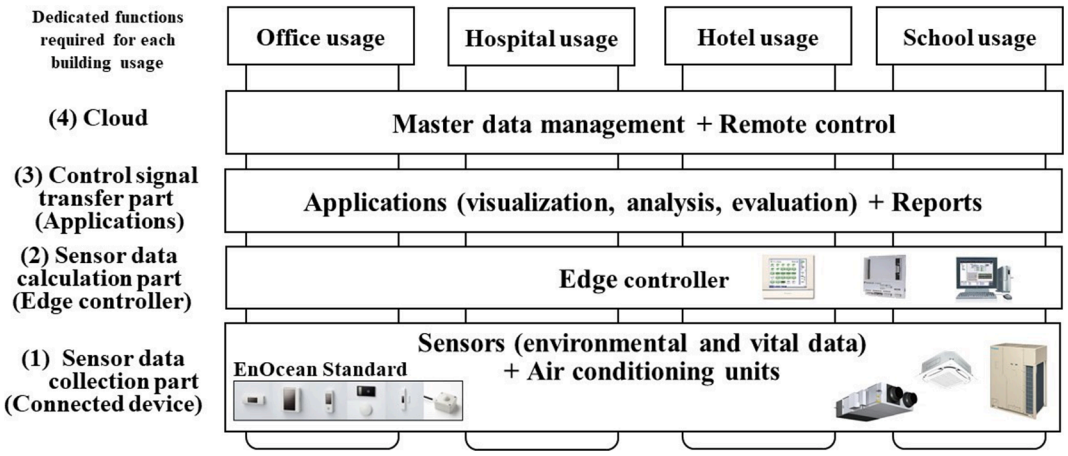

Fig. 2. System architecture chart.

Table 1
Command summary.

Command	Function name	Function
Get unit information	GetUnitInfo	Acquiring indoor unit and outdoor unit information individually, or all unit information collectively.
Set Indoor unit operation	SetIuStatus	Setting indoor unit operation mode (e.g., start/stop and set temperature).

Table 2
Parameters for indoor unit.

Unit	Item	Content	
Indoor −Unit	Unit-ID		Unique ID assigned to each device
	Attribute	Name	Installed unit name
		Address	Address
	Unit status	Status	Normal/ Unit error/ Communication error
		Error	Error code
		On/Off Status	On/ Off/ Unknown
		Operation Mode	Cooling/ Heating/ Fan/ Dry/ Automatic
		Suction temperature	One decimal place (−50.0 ℃–100.0 ℃)
		Setpoint temperature	One decimal place (15.0 ℃–35.0 ℃)
		Flow rate	Low/ Middle/ High
		Flow direction	5 directions + Swing

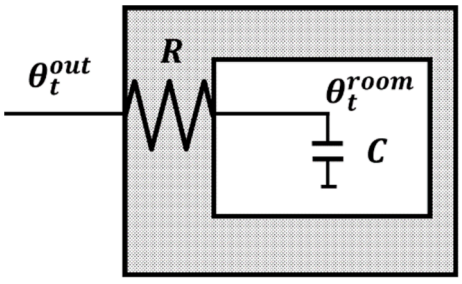

Fig. 3. CR model used in analysis.

indoor units.

It has been found that system operation via remote control operation can lead to energy loss due to suboptimal temperature settings (e.g., excessively high or low temperature settings and failure to turn off equipment at appropriate times). Furthermore, VRF equipment is selected based on the maximum load expected in the room in which it is installed, but this maximum load only occurs for a limited number of hours per year. As a result, the equipment has been found to operate for many hours at a low load factor, which reduces the efficiency of the equipment [27].

In this study, a system was developed that operates both indoor and outdoor units based on the properties of room air (e.g., temperature, humidity, air velocity, and human flow). These properties are measured using external sensors. By optimizing the type, number, and placement of sensors, it is feasible to design a VRF system that operates independent of remote control.

The system comprises a cost-effective VRF setup equipped with wireless sensors and an edge server running on a Linux platform. The integration of wireless sensors allows for the addition of various sensors at subsequent stages. The edge server is responsible for collecting sensor data, performing calculations, and transmitting signals *via* HTTP to the air conditioner controller. The system is designed to be simple, economical, and adaptable. We demonstrate that the system can maintain comfortable and automatic energy-efficient operation through four types of control, eliminating the need for manual intervention with a remote control.

The controls include pre-cooling and pre-heating based on outdoor and indoor temperatures, air conditioning output capacity, and power consumption; human detection ventilation control that integrates image-type human flow sensors with indoor units; a rotational control strategy for outdoor units to enhance efficiency in areas with low demand; and a fan power reduction control that ceases the operation of all indoor VRF units once the set temperature is achieved. The findings of remote-control-free VRF system testing are presented and discussed. We present a highly important technology that contributes to the widespread adoption of smart buildings.

2. Methods

The study was conducted in five stages:

(1) Definition of switchless control and determination of functional specifications.
(2) Design and development of a switchless control system, including hardware and data flow.
(3) Design and implementation of system functions.
(4) Preparation of the target classroom for the demonstration experiment and design of the experiment, including the number and location of sensors.
(5) Analysis and interpretation of the results.

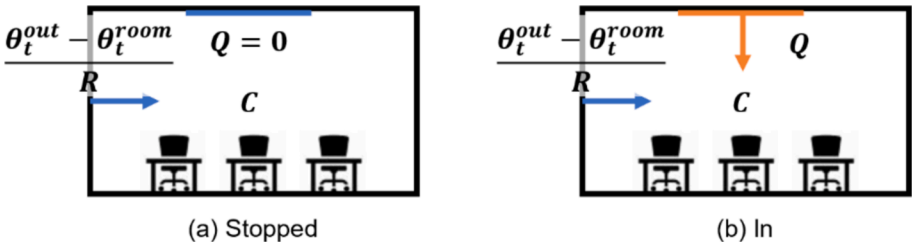

Fig. 4. CR model used in analysis.

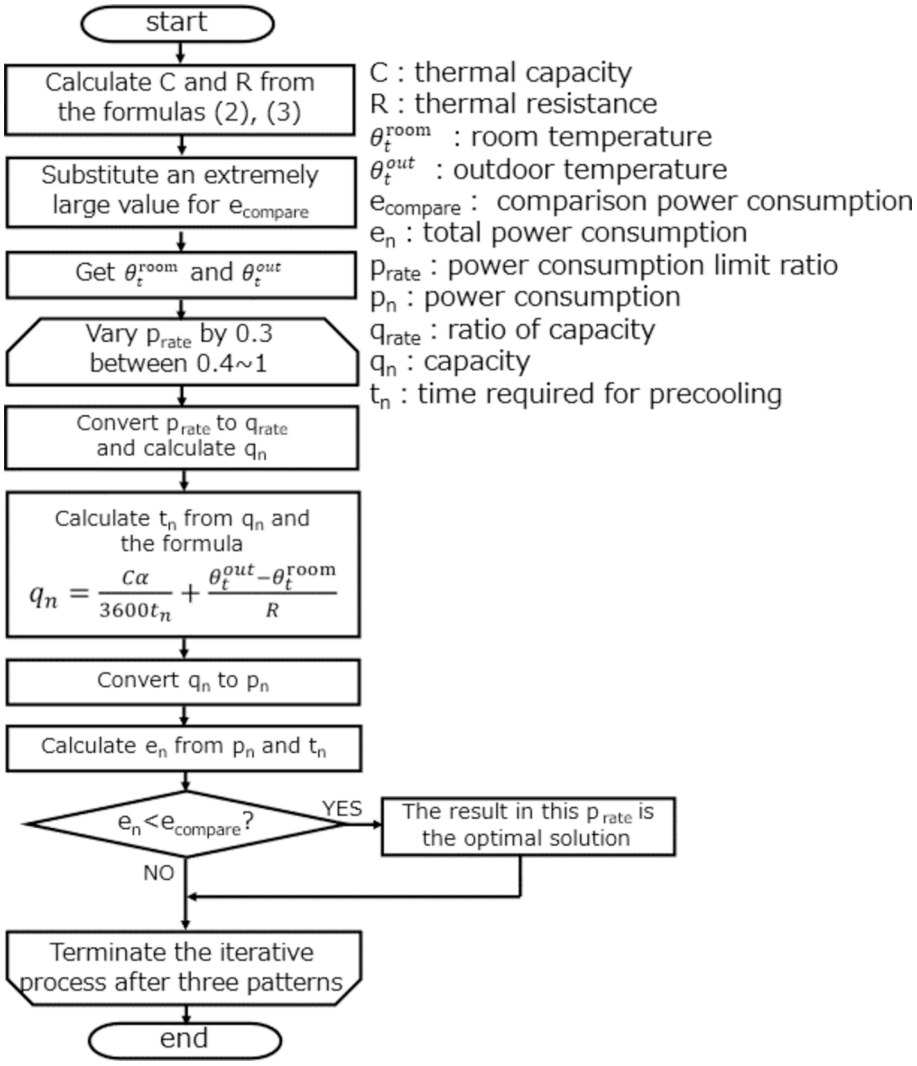

Fig. 5. Pre-cooling and pre-heating functions.

The following sections provide detailed descriptions of these stages.

2.1. Definition of switchless control for VRF system

A switchless air-conditioning system is a fully automated system that operates without manual switch intervention. It intelligently adjusts the environmental conditions (e.g., temperature, humidity, and airflow) based on anticipated movements and changes within the space, thereby creating a smart space that is both energy-efficient and comfortable.

The objectives of such a system are as follows:

(1) Ensuring minimal energy consumption during operation.
(2) Maintaining a comfortable indoor environment by eliminating manual control by individual users.
(3) Managing energy consumption on a per-occupant basis.

A switchless air-conditioning system comprises sensors that measure environmental properties (sensing functions) and software that controls air-conditioning and ventilation (actuator functions) based on sensor data. These sensors can detect a variety of spatial and environmental factors, including temperature, humidity, wind speed, atmospheric pressure, CO_2 level, illumination, odor, dust, human presence, and the status of openings (open/closed).

Actuator functions encompass settings typically adjustable via an air

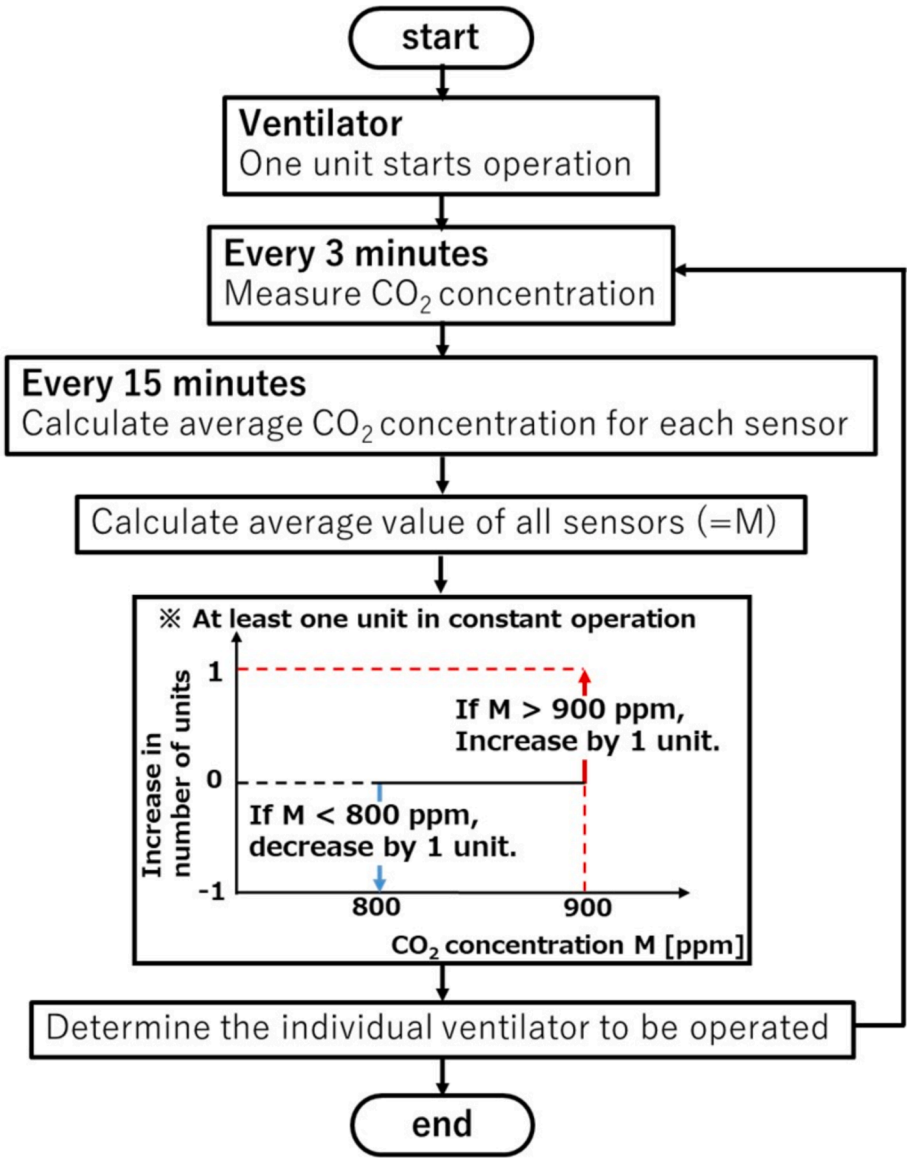

Fig. 6. CO_2 control function.

conditioner remote control (on/off, mode selection such as cooling, heating, dry or blast, temperature control, air volume, and air direction with options of fixed or swing). Additionally, the settings applicable to the ventilation system are included. The system enables air conditioning control based on indoor and outdoor temperature and humidity data, as well as air conditioning and ventilation control informed by human detection and CO_2 level.

2.2. System configuration and dataflow

The configuration of the switchless air-conditioning system is illustrated in Fig. 1, which collects sensor data, performs calculations, and transmits signals via HTTP to an air-conditioning controller. The system utilizes environmental sensors equipped with solar power, eliminating the need for external power or wiring, and forms a wireless sensor network.

The system architecture is illustrated in Fig. 2, which is organized into four tiers (1)-(4). This hierarchical structure facilitates the addition of hardware and software components. The functions can be modified, and thresholds adjusted based on the specific requirements of the building.

Wireless sensors in the system harvest energy from environmental sources such as motion, light, and temperature to power their wireless communications. Sensor data are acquired through receivers and processed by edge servers, which also serve as IoT gateways. These servers perform adjustments on the collected sensor data. The control software employs the open-source programming tool Node-RED, which allows for easy expansion and helps reduce development costs. The processed data are then transmitted from the edge server to the central controller of the air conditioner.

To alter the operational state of the indoor units and ventilators, which function as actuators, the edge server sends control variables to the central controller via HTTP, based on the processed data. This interaction involves generating and sending request and response commands. Specifically, an HTTP request is made using the GET method, and responses are received in XML format. The basic format of the request command is as follows:

http://<IP address of central controller>/WebService/<Optional command>.

Communication between the wireless sensor and Node-RED is facilitated by the IPC-in node of Node-RED, which receives input from Linux domain sockets and converts it into data or events, and the JSON

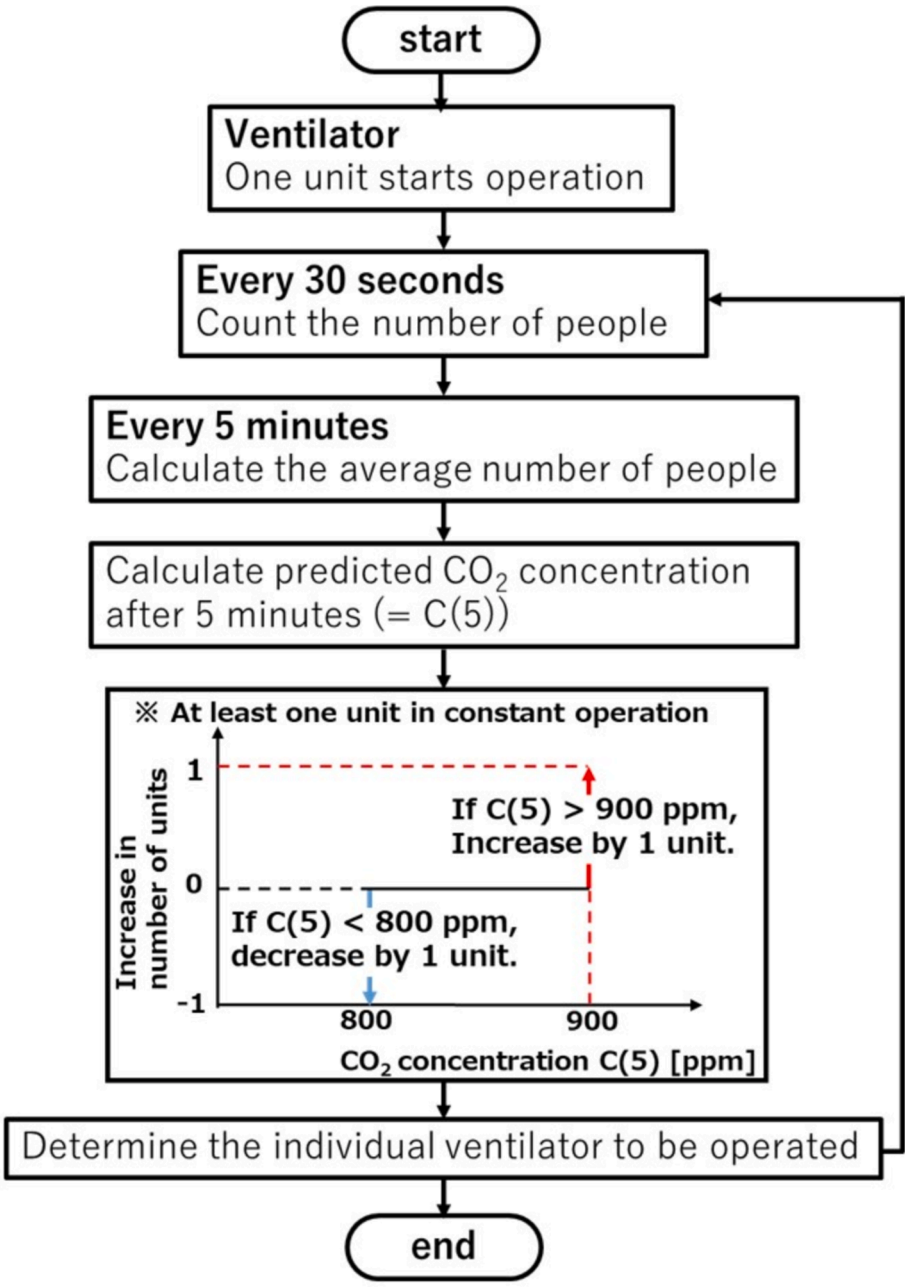

Fig. 7. Human detection control function.

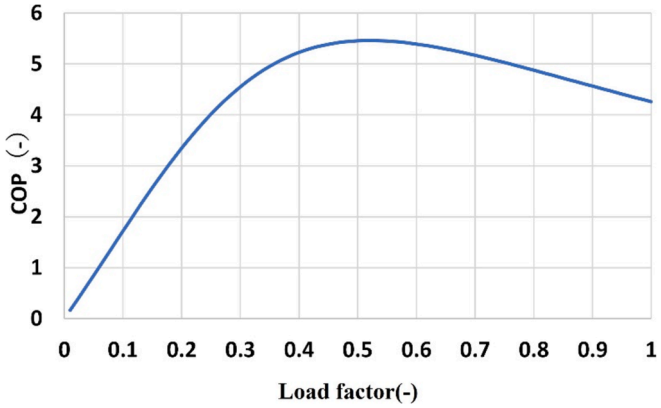

Fig. 8. Performance curve (cooling).

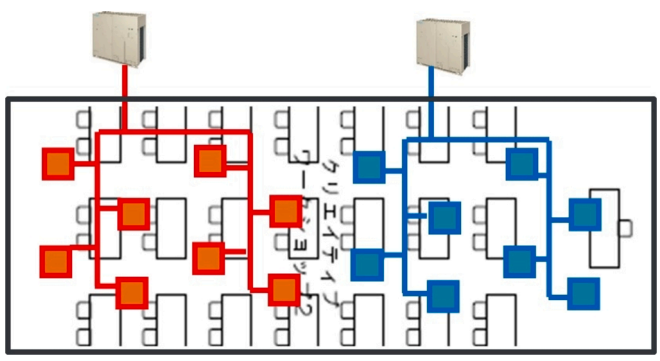

Fig. 9. VRF indoor unit placement.

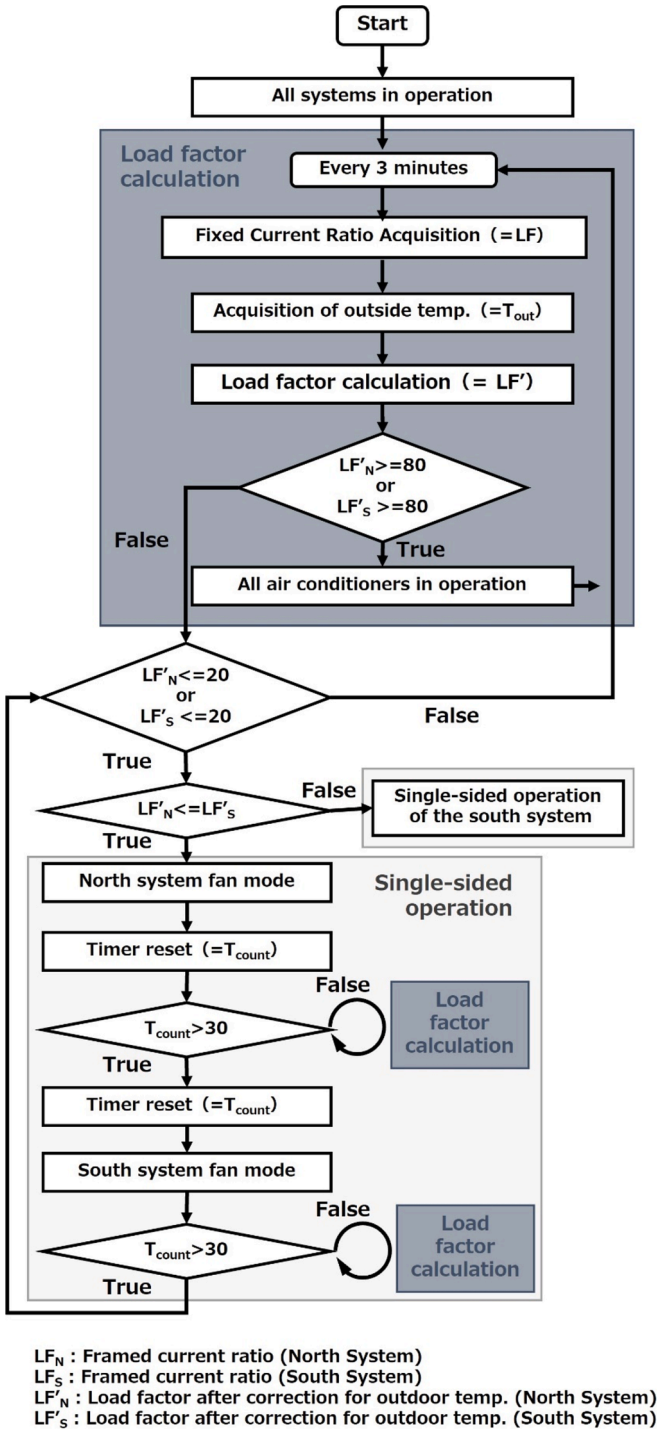

Fig. 10. Control flow of rotation control.

node, which formats sensor data into JSON for processing by Node-RED. For communication between the edge server and the PC used for data analysis, the websocket-out node is employed on the sender's side and the websocket-in node on the receiver's side. Additionally, a file node on the PC is utilized to create arbitrary management files.

Two command requests can be set for the central controller: equipment information acquisition and indoor unit operation settings, as outlined in Table 1. The equipment information acquisition command allows for the retrieval of data specified in Table 2 for indoor units and the acquisition of performance coefficients and capacity values for outdoor units. This command primarily assesses the status of indoor

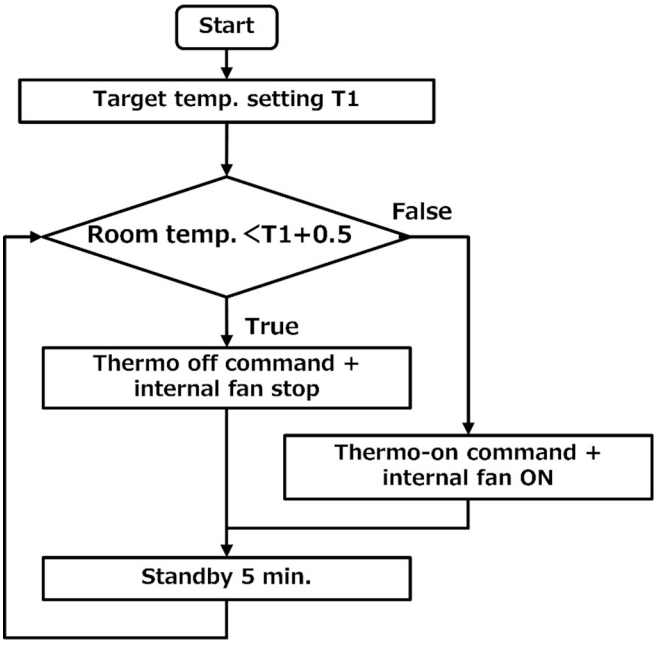

Fig. 11. Control flow of fan power reduction function.

units. The indoor unit operation setting command is crucial for utilizing an indoor unit as an actuator, enabling switchless control through a combination of these methods.

2.3. Switchless control function

This section details the four switchless air conditioning control functions developed:

2.3.1. Pre-cooling and pre-heating function

This function is designed to minimize energy consumption by calculating the thermal resistance (R) and thermal capacity (C) of a room using the air conditioner's equipment status and external sensors (temperature and humidity). It then determines the optimal start time (T_s) for air conditioning and the appropriate air conditioning output capacity (P_{rate}), which varies for cooling and heating, based on these sensor values.

In the CR model, which draws from thermal circuit theory, the heat balance is analogous to an electrical circuit with components including a thermal resistor and capacitor, as illustrated in Fig. 3. A diagram of the heat balance in the CR model is illustrated in Fig. 4(a). The model can be simplified by neglecting internal heat generation and other factors when the air conditioning is off, expressed with the following equation:

$$C\frac{d\theta_t^{room}}{dt} = \frac{-(\theta_t^{room} - \theta_t^{out})}{R}; \quad (1)$$

where, t represents time index and θ_t^{room} and θ_t^{out} denote room temperature and outside temperature at time t, respectively. Assuming the outside temperature remains nearly constant, the equation simplifies to

$$\theta_t^{room} - \theta_t^{out} = \left(\theta_0^{room} - \theta_0^{out}\right) e^{\frac{-t}{CR}}. \quad (2)$$

The C–R values were estimated using the least-squares method considering the data obtained when air conditioning was not in use for two consecutive hours.

The values of C and R were then calculated separately based on the changes in outdoor and room temperatures during the first 2 h of air conditioning operation and the amount of heat processed by the air conditioning system during this time. This analysis is depicted in Fig. 4 (b).

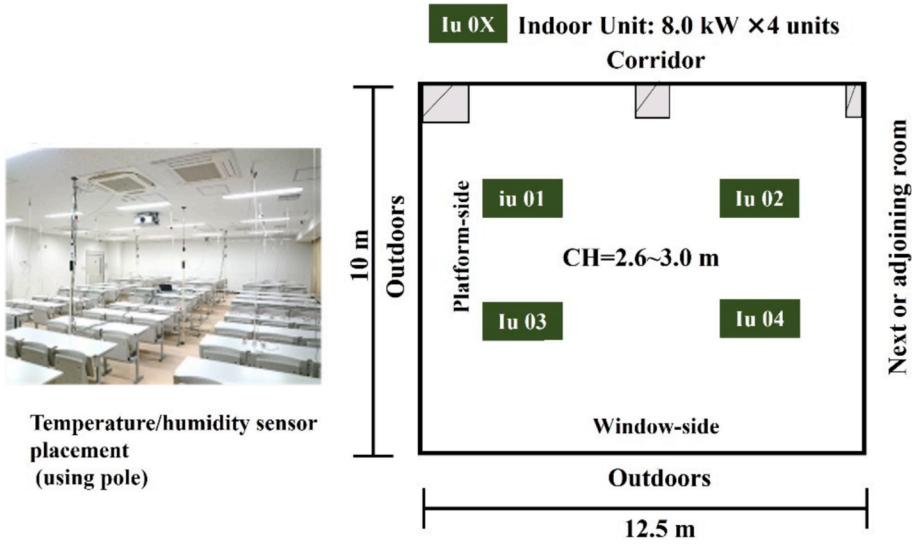

Fig. 12. Images and diagram of lecture room 1.

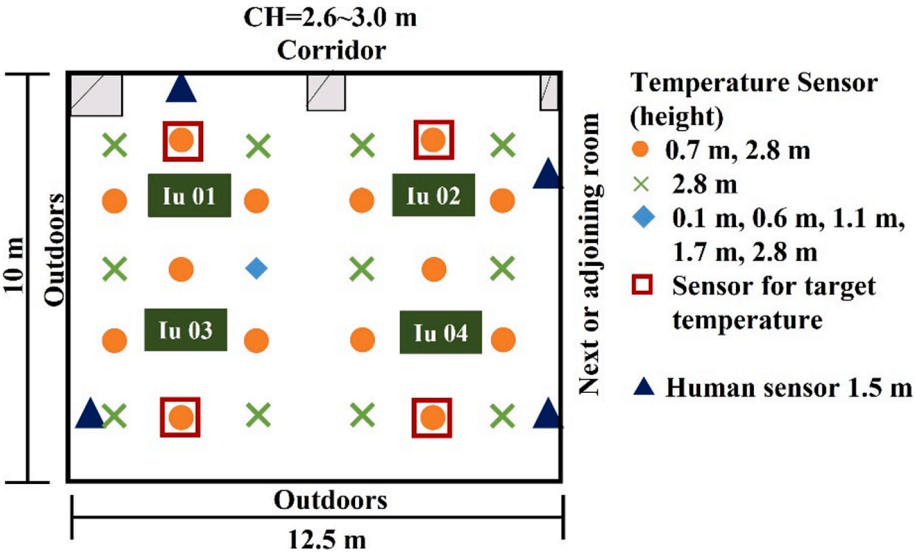

Fig. 13. Locations of sensors in lecture room 1.

$$C\frac{\Delta\theta_t^{room}}{\Delta t} = \frac{\theta_0^{out} - \theta_t^{room}}{R} + Q. \quad (3)$$

First, the energy consumed to achieve the set temperature was estimated for scenarios where the air conditioner operated at 40 %, 70 %, and 100 % of its maximum capacity. After identifying the capacity that consumed the least energy among these conditions, the time needed to reach the set temperature at this optimal capacity was calculated, and the pre-cooling start time was established. A flow diagram of this process is illustrated in Fig. 5. This approach minimizes energy consumption by adjusting the start time and air-conditioning capacity according to the thermal characteristics of the room and the outdoor temperature on the day. The moment when the set temperature was achieved marked the beginning of the class (conducted in lecture rooms).

2.3.2. *Human sensing HVAC control function*

This system also includes a function to detect the presence or absence of people, aiming to minimize ventilation and enhance energy efficiency by reducing the ventilation load. To ascertain whether people were present, two methods were evaluated: monitoring changes in CO_2 concentration (using a CO_2 sensor) and employing an image-based human flow sensor. The control flows for these methods are depicted in Figs. 6 and 7. This feature was specifically implemented to conserve energy in ventilation systems during classes.

2.3.3. *Outdoor unit rotation control function*

Generally, a VRF system displays the performance characteristics illustrated in Fig. 8 under constant outdoor temperatures (as per the National Research and Development Agency, Building Research Institute, and Energy Consumption Calculation Program for Buildings (Nonhousing Version)).

Fig. 8 indicates that peak efficiency was achieved at a load factor of approximately 0.5, and efficiency significantly decreased at extremely low load factors, particularly below 0.2. In scenarios involving a living room with multiple indoor units connected to several outdoor systems (as depicted in Fig. 9), each indoor unit manages the load for its designated zone. However, during periods of low demand, frequent cycling of the thermo-on/off occurs, leading to inefficient operation. Additionally, the selection of indoor and outdoor units with capacities larger than necessary contributes to this inefficiency. To enhance efficiency, a

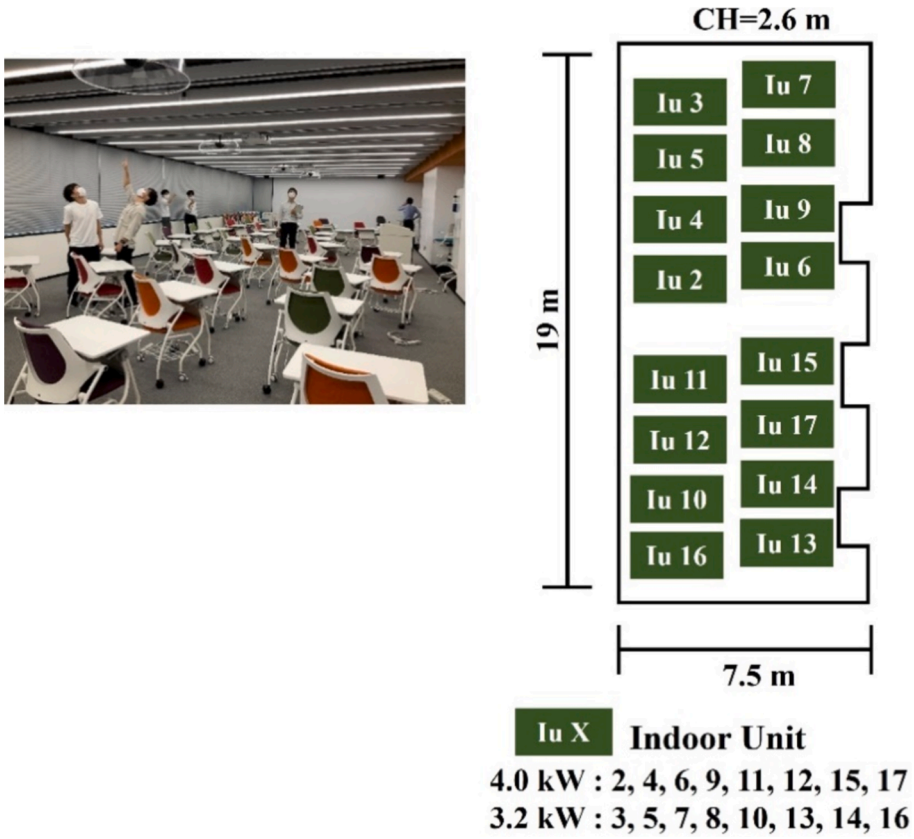

Fig. 14. Images and diagram of lecture room 2.

control strategy that involves rotating the operation of outdoor units was implemented. This rotation control function allows for high COP operation while maintaining uniform indoor conditions by alternating load processing and air blowing operations across the systems. The control flow for this strategy is illustrated in Fig. 10.

2.3.4. *Indoor unit fan power reduction function*

The fan of the indoor unit in the VRF system was programmed to remain operational even when the thermostat was deactivated. This operational mode was necessitated by the room temperature being monitored via a temperature sensor located within the indoor unit, which prevented the fan from being turned off. Consequently, a separate sensor was installed to measure the room temperature, enabling control over the fan power of the indoor unit during periods when the thermostat was off. This control mechanism is depicted in Fig. 11.

2.4. *Lecture room and sensor layout for demonstration*

The experiment was conducted in two university lecture rooms. Lecture Room 1, detailed in Fig. 12, measures 10 m × 12.5 m with a ceiling height of 2.8 m. It is equipped with four indoor units, each having a cooling capacity of 8.0 kW, spaced approximately equidistantly. Each set of four indoor units is served by one outdoor unit. The wall behind the teaching platform, which lacks windows, faces the exterior. The right wall, as viewed from the platform, also faces the exterior and includes windows, while the left wall adjoins an unconditioned corridor. The wall opposite the platform abuts another air-conditioned room. The placement of temperature and humidity sensors within this room is illustrated in Fig. 13, with sensor positions marked by circles. The sensor distribution is color-coded: green for one sensor at 2.8 m, red for two sensors at 0.7 and 2.8 m, and blue for five sensors at heights of 0.1, 0.6, 1.1, 1.7, and 2.8 m.

Lecture Room 2 is outlined in Fig. 14, with dimensions of 19 m × 7.5 m and a ceiling height of 2.6 m. It contains 16 indoor units, each with a cooling capacity of either 3.2 or 4.0 kW, installed at regular intervals. The left wall, which includes a window, faces the outdoor. Adjacent to the right wall is a corridor, and the remaining walls are contiguous with other rooms. The locations of the temperature and humidity sensors in this room are shown in Fig. 15, with sensor types indicated by colored circles: orange for temperature and humidity sensors, green for CO_2 sensors, and blue for image-based human flow sensors capable of counting people. The outcomes of the experiments conducted in these lecture rooms are summarized in Table 3.

3. Results and discussion

Here, we discuss the outcomes of automated air-conditioning operations using the VRF system.

3.1. *Results of pre-cooling and pre-heating operation*

A pre-cooling operation adhering to a predefined cooling schedule was conducted in lecture room 1 from July 20, 2021, to July 27, 2021. The experiments were carried out under three different energy consumption limits: no limit, 40 % limit, and 70 % limit. The duration from the commencement of operation at 05:00 to the point when the set temperature was achieved, along with the energy consumption and peak energy consumption, was analyzed. The load factor, rated energy consumption ratio, room temperature, and outdoor air temperature for the three scenarios are depicted in Figs. 16, 17, and 18.

In the scenario with no limit (Fig. 16), the rated energy consumption ratio reached 120 % of the peak value shortly after the operation commenced. Subsequently, the load factor decreased gradually as the room temperature dropped, achieving a set temperature of 23 °C at 05:47. In the 70 % limit scenario (Fig. 17), the cooling capacity was approximately 80 % because the energy consumption ratio was

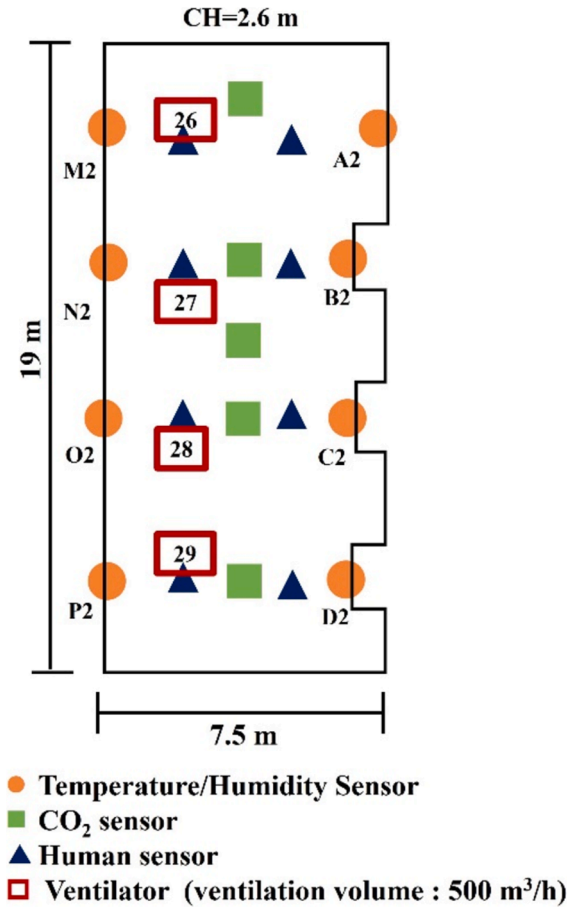

Fig. 15. Locations of sensors in lecture room 2.

Table 3
Tests carried out in lecture rooms.

Function	Experiment	Location
Pre-cooling and pre-heating	Pre-cooling and pre-heating	Lecture room 1
	Winter pre-heating	Lecture room 2
Human detection ventilation control	Winter heating	Lecture room 2
Rotation control	Summer cooling	Lecture room 2
Reduction of fan power	Winter heating	Lecture room 2

restricted to 70 % from the start. After about 25 min of operation at 80 %, the load ratio decreased as the room temperature neared the set temperature, which was maintained at 05:48. In the 40 % limit scenario (Fig. 18), the energy consumption ratio was consistently held at 40 % from the start until the set temperature was reached at 05:59. At around 05:45, when the outdoor air temperature was higher, the energy consumption ratio remained at 40 %, but the load factor decreased by approximately 6 % owing to the reduced efficiency of the air conditioner.

The results of these tests are summarized in Table 4. The no control and 70 % limit conditions consumed 18 % more power than the 40 % limit condition, with the 40 % condition consuming the least amount of power. The COP was also the highest for the 40 % limit condition, as expected.

The pre-heating operation test during the heating season was conducted from December 14, 2021 to February 3, 2022. The results of these tests, in which the outdoor air temperatures were similar, are shown in Table 5. For similar outdoor temperature conditions, the pre-heating time was in the order of 40 % limit >70 % limit > no control. The heating time for the 40 % limit was approximately twice that of the no control. The highest energy consumption was observed in the no-control condition among these three cases. The uncontrolled condition resulted in a 21 % increase in energy consumption compared to the 40 % limit condition. The 40 % limit condition resulted in the lowest energy consumption during the pre-heating operation condition as well as the pre-cooling operation condition.

The pre-heating control logic was implemented in lecture room 2 on the edge server from February 26–27, 2023 during the winter pre-heating operation. The results are presented in Fig. 19. The class was scheduled to start at 08:50, which was set as the target time for initiating the pre-heating control. According to the CR calculations, the pre-heating operation commenced automatically at 07:45, 1 h and 5 min before the class began, with an energy consumption limit of 40 %. In contrast, without the pre-heating control, the heating system activated automatically 30 min before the class based on a scheduled control. The total energy consumption was evaluated from the start of the operation until 10:00. With the pre-heating control, energy consumption was 8.2 kWh, compared to 9.2 kWh without control, reflecting an 11 % reduction in energy usage. Additionally, energy efficiency improved, and the indoor temperature was higher than that in the scenario without control. The outdoor temperatures on the days compared were similar from early morning until 10:00.

3.2. *Results of human detection ventilation control*

The effectiveness of the ventilation control was assessed in the same lecture room from January 19, 2022 to January 26, 2022 using the methods described above. The findings are illustrated in Figs. 20, 21, and 22. Without ventilation control (Fig. 20), the four ventilation

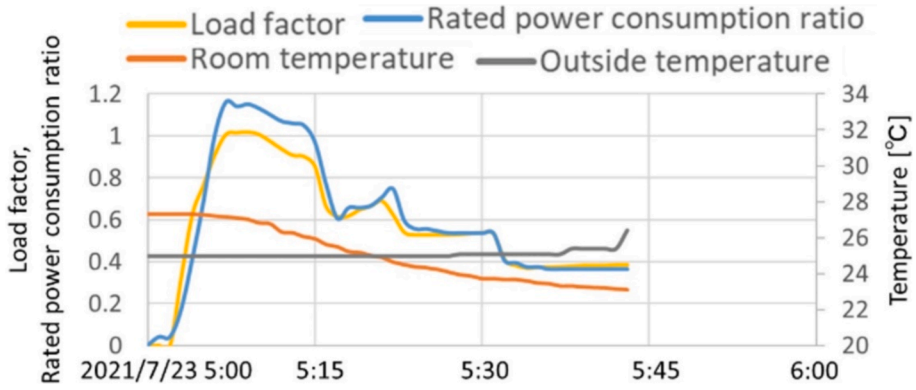

Fig. 16. Changes in load factor without control.

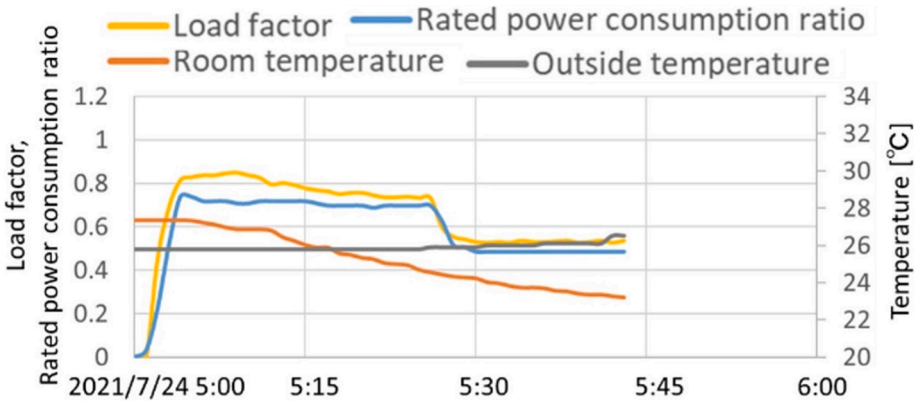

Fig. 17. Changes in load factor for 70 % limit.

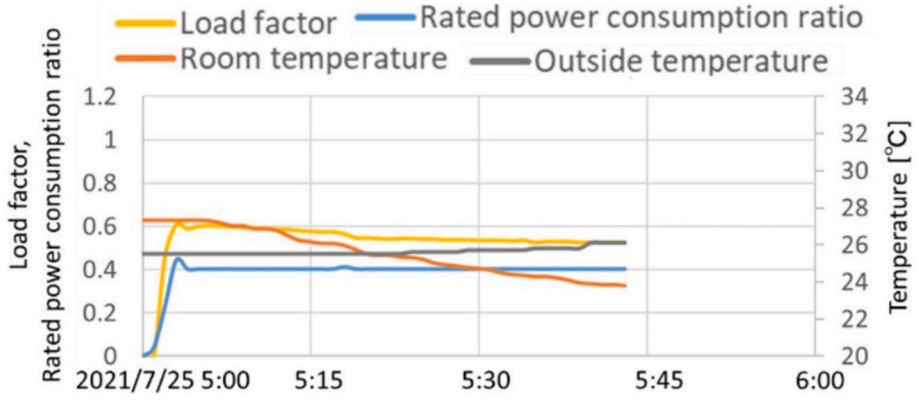

Fig. 18. Changes in load factor for 40 % limit.

Table 4
Pre-cooling operation results. (COP: coefficient of performance; AOT: average outdoor temperature).

Energy consumption ratio	Date	COP [-]	Electrical energy [kWh]	Pre-cooling time [m]	AOT [°C]
No control	7/23	3.24	4.6(1.18*)	47	25.1
70 %	7/24	3.75	4.6(1.18*)	48	26.0
40 %	7/25	4.48	3.9 (1.00*)	59	25.9

*Percentage with 40% as 1.0.

Table 5
Pre-heating operation results. (COP: coefficient of performance; AOT: average outdoor temperature).

Energy consumption ratio	Date	COP [-]	Electrical energy [kWh]	Pre-heating time [m]	AOT [°C]
No control (trial 2)	2/3	2.67	5.8 (1.21*)	38	4.0
70 % (trial 1)	12/15	3.16	5.0 (1.04*)	46	4.0
40 % (trial 1)	12/14	3.19	4.8 (1.00*)	77	4.0

(*Percentage with 40% as 1.0).

devices operated continuously, generating a total airflow of 2000 CMH. According to the Japanese standard, the required ventilation volume per person is 30 CMH. With a maximum occupancy of approximately 25 people (as indicated by the green line in the diagram, measured using an image-type human flow sensor), a ventilation volume of 750 CMH would suffice. The maximum CO_2 concentration reached 650 ppm (red line in the diagram), suggesting excessive ventilation.

With ventilation control (Fig. 21), the CO_2 concentration (red line) increased as the number of occupants (green line) grew, starting around 10:30 when the class began. The number of operational ventilation units adjusted accordingly but with a delay, leading to a peak CO_2 concentration of 1000 ppm around 11:30. The subsequent increase in ventilation volume helped reduce CO_2 level. A similar adjustment occurred around 15:00. These controls facilitated energy-efficient ventilation management.

In the experiment involving an image-based human flow sensor for ventilation control (refer to Fig. 22), the number of ventilation units was adjusted by one unit in response to each increase or decrease in the number of people, demonstrating a direct correlation with changes in CO_2 level. This method exhibited a faster control response compared to CO_2 control.

The average outdoor air temperature during the experimental period is comparatively plotted with the total energy consumption of the air conditioning and ventilation systems under different conditions in Fig. 23. The data indicate that both CO_2 control and human detection control methods reduced electrical energy consumption by approximately 35 % compared to the baseline.

3.3. Result of outdoor unit rotation control

During the period from September 12 to 29, 2022, rotational control

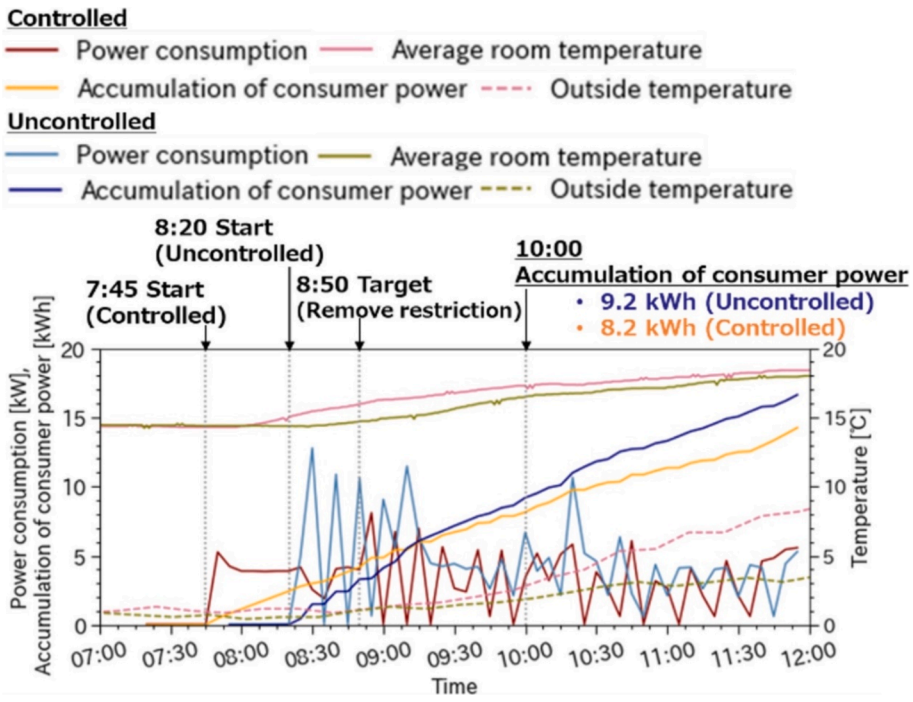

Fig. 19. Pre-heating operation results.

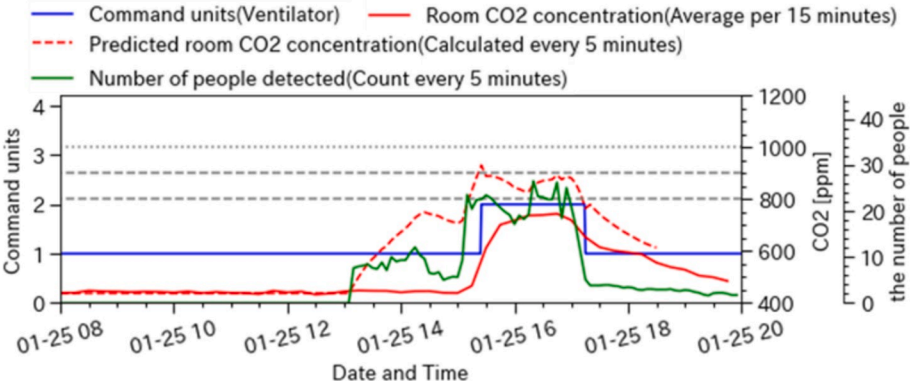

Fig. 20. Results obtained without sensor control.

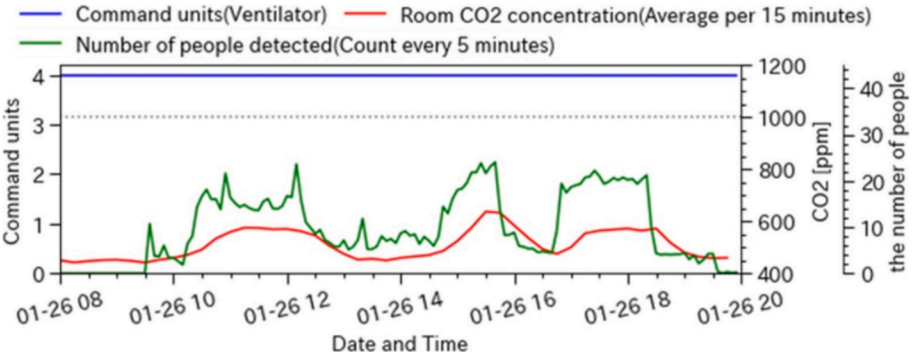

Fig. 21. Results obtained with CO_2 control.

of the outdoor unit was tested in demonstration lecture room 2. Fig. 24 illustrates the relationship between the load factor and COP of the southern system during this period, with additional details provided in Table 6. In the absence of control, the load factor consistently ranged between 0.1 and 0.2, as the compressor operated primarily in the start/stop region. Furthermore, when the compressor was thermally activated, it operated at the lowest frequency, resulting in an average evaporation temperature of 8.4 °C and a low COP of 3.15, as depicted on

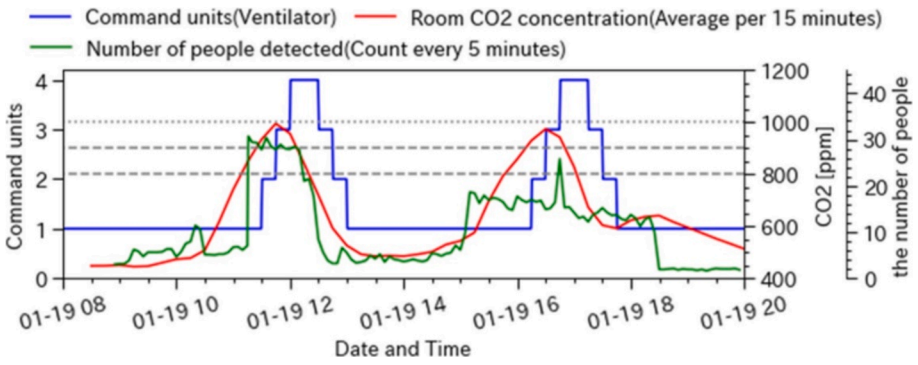

Fig. 22. Results obtained with human detection control.

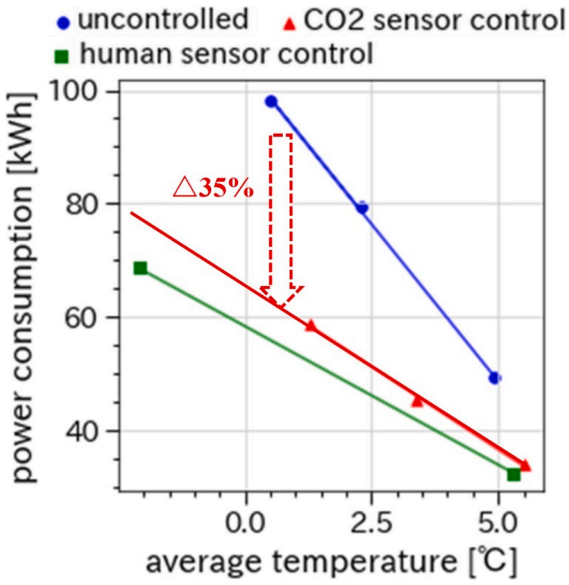

Fig. 23. Comparison of three types of ventilation control.

the left side of Fig. 25.

Conversely, with the implementation of rotational control, both systems were active for 30 min/h. Although the load factor depicted in Fig. 24 remained between 0.1 and 0.2, which is similar to the scenario without control, the actual operational load factor effectively doubled to approximately 0.2 to 0.4 for those 30 min. Consequently, as shown on the right side of Fig. 25, the COP improved to 3.71, corresponding with an increase in evaporation temperature to 10.7 °C, marking an enhancement of 17.7 %.

In one of the outdoor unit systems, fan operation was controlled rotationally, raising concerns about a potential increase in room temperature on the thermo-off side. To investigate this aspect, we examined the temperature history of a room with and without rotational control (Figs. 26 and 27; sensor positions labelled as A2 in Fig. 15). The results depicted in Fig. 26, without rotational control, exhibited minimal temperature fluctuations at each sensor location. Conversely, Fig. 27, with rotational control, exhibited temperature variations of approximately 0.5 °C in a 1-h cycle because of the 30-min airflow operation time. Despite these fluctuations, it was confirmed that the indoor temperature generally remained around 24 °C, consistent with the scenario without rotational control.

3.4. Results of fan power reduction control

Fig. 28 illustrates the operation times for thermo-on and thermo-off of the indoor units from January to December 2023 in demonstration lecture room 2. The thermo-off time constituted 67.6 % of the total operating time, indicating prolonged periods of inactivity. Table 7 details the power consumption of both outdoor and indoor units during this period. Despite the indoor unit being a low-power cassette-type, it

Table 6
COP and load factor results.

	COP (–)	Load factor (–)	Evaporation temp. (℃)
No rotation	3.15	0.13	8.4
With rotation	3.71 (17.7 %up)	0.12	10.7

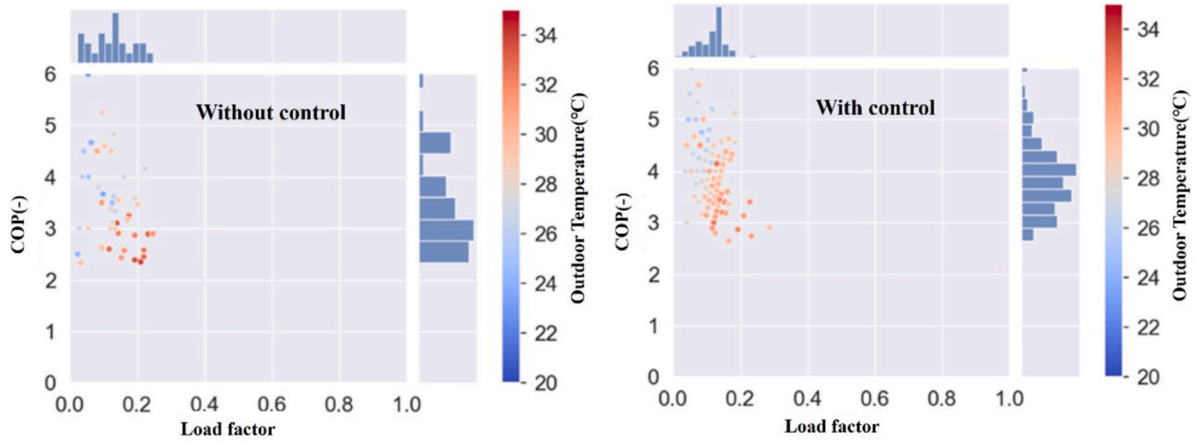

Fig. 24. COP with and without rotation control (hourly average value).

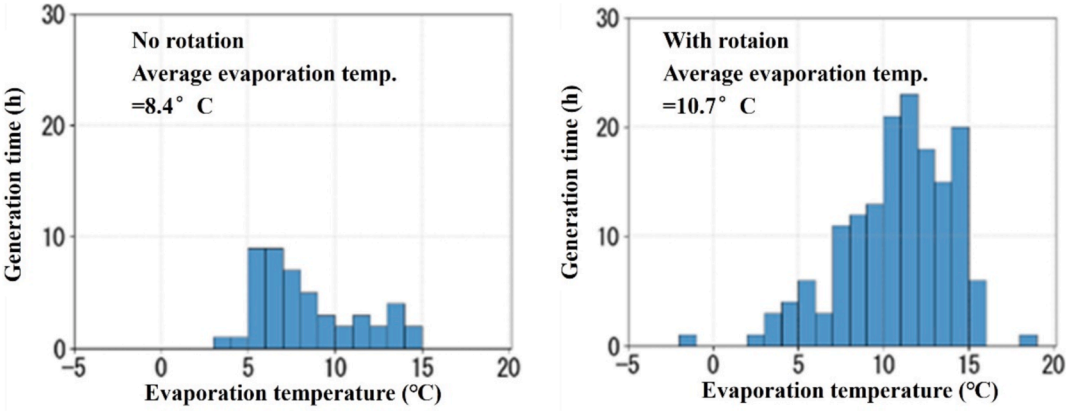

Fig. 25. Comparison of evaporation temperature occurrence frequency.

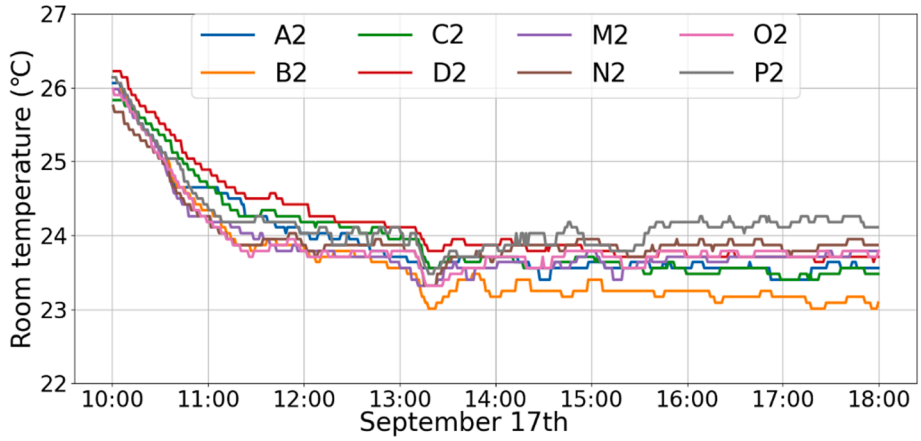

Fig. 26. Indoor temperature (without rotation).

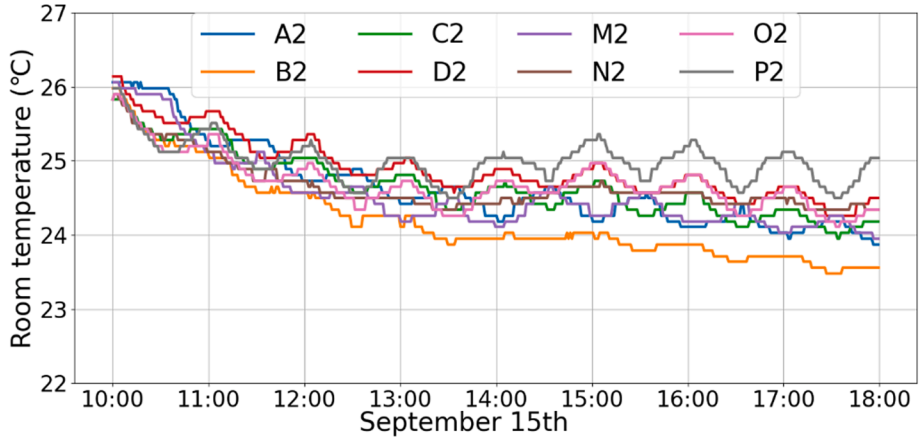

Fig. 27. Indoor temperature (with rotation).

accounted for 9.9 % of the total power consumption. Thus, reducing the fan power during thermo-off could potentially decrease power consumption by 9.9 % × 67.6 % = 6.7 %.

Fig. 29 presents the results of a demonstration conducted from February 28 to March 11, 2024, alternating between settings with and those without rotational control. Comparing March 7 and 8, which had similar outdoor temperatures (indicated with a red dotted line in the figure), the thermo-on times were roughly equivalent. However, the fan operation time during thermo-off was reduced by 81.1 %. The power consumptions during this period are listed in Table 8. The fan power of the indoor unit, which originally constituted 18.9 % of the total power consumption, was reduced to 8.6 % through this control. Additionally, by stopping the indoor unit fan, fine heating (*) was minimized, and the power consumption of the outdoor unit was simultaneously reduced, achieving an overall reduction of 26.5 %.

(* Operation to suppress refrigerant accumulation in indoor units).

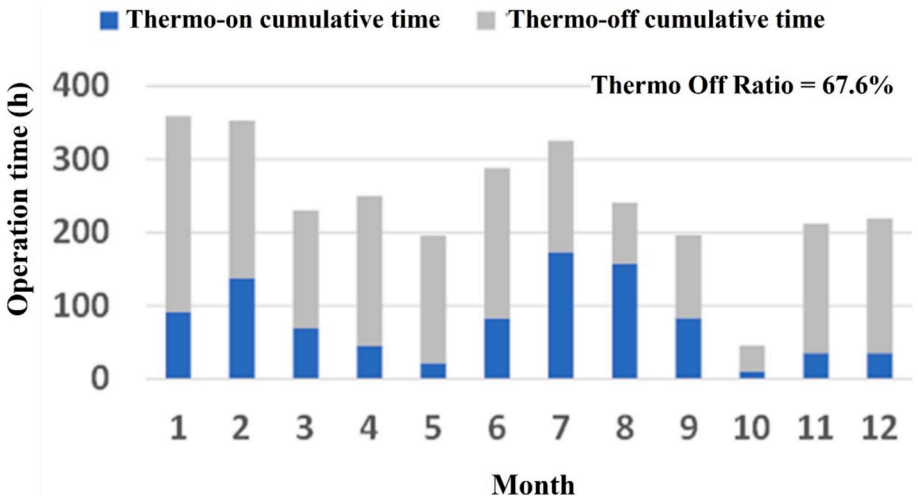

Fig. 28. Indoor unit thermo-on and thermo-off operation time.

Table 7
Annual power consumption.

Classification	Power consumption [kWh]	Percentage
Outdoor unit	8493.9	90.1 %
Indoor unit	937.5	9.9 %

4. Conclusion

In this study, a switchless VRF system was developed and evaluated based on four key functionalities:

1. During the initial pre-cooling and pre-heating operations, the VRF system demonstrated significant energy efficiency, achieving 18 % energy savings in summer pre-cooling. In winter pre-heating, it accomplished 21 % energy savings.
2. The human-detection ventilation control effectively modulated the ventilation volume by real-time monitoring of the number of occupants, resulting in approximately 35 % energy savings without compromising thermal comfort.
3. The rotational control strategy enhanced the average COP of the outdoor units by 17.7 %. This was achieved by operating one of the outdoor units in the fan mode during periods of low demand, whereas the other remained in the cooling mode.
4. A reduction in indoor-unit fan power led to an overall power consumption decrease of 8.6 % by ceasing fan operation when the thermostat was deactivated.

The findings confirm that the switchless control VRF system effectively maintains comfort while reducing energy consumption. Previously, operation was conducted using remote controls installed in each room, which often resulted in improper operation. However, by utilizing the method presented in this study, it is possible to prevent such improper operation while efficiently achieving the desired indoor environment. Furthermore, this method can be applied even when various air-conditioning layouts and sensor placements are freely modified. This system will become a highly important technology in accelerating the smart building transformation of small and medium-sized buildings.

Table 8
Power Consumption.

Classification	Mar. 7	Mar. 8
Outdoor unit power consumption [kWh]	15.4	12.7
Indoor unit power consumption [kWh]	3.5	1.2
(Indoor power/total power)	(18.9 %)	(8.6 %)
total amount [kWh]	18.9	13.9
Reduction ratio	–	26.5 %

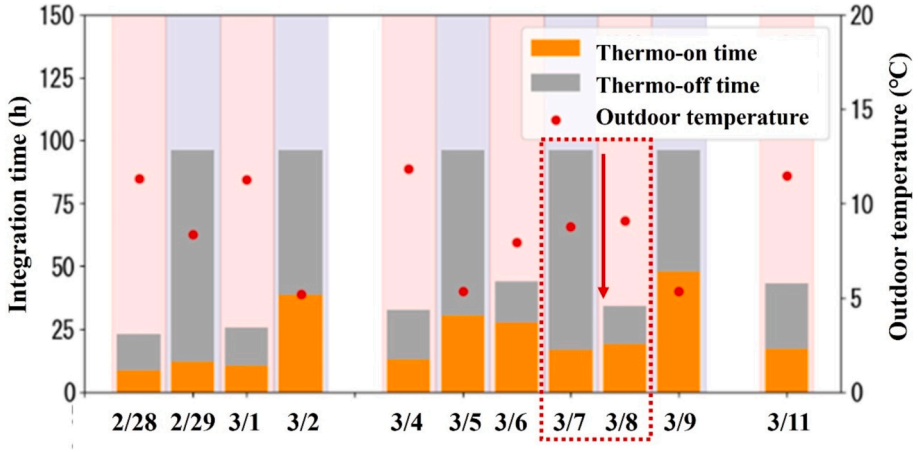

Fig. 29. Results of fan power reduction control.

CRediT authorship contribution statement

Toshihiro Suzuki: Writing – review & editing, Writing – original draft, Validation, Supervision, Project administration, Methodology, Conceptualization. **Yoshiyuki Shimoda:** Supervision, Conceptualization. **Akito Kobayashi:** Visualization, Formal analysis, Data curation. **Sumio Shiochi:** Supervision, Conceptualization.

Declaration of competing interest

The authors declare that they have no known competing financial interests or personal relationships that could have appeared to influence the work reported in this paper.

Data availability

Data will be made available on request.

References

[1] IEA, World energy outlook 2022, IEA, Paris. https://www.iea.org/reports/world-energy-outlook-2022, 2022. (accessed 5 October 2024).

[2] Y. Bae, S. Bhattacharya, B. Cui, S. Lee, Y. Li, L. Zhang, P. Im, V. Adetola, D. Vrabie, M. Leach, T. Kuruganti, Sensor impacts on building and HVAC controls: a critical review for building energy performance, Adv. Appl. Energy. 4 (2021) 100068, https://doi.org/10.1016/j.adapen.2021.100068.

[3] M. Gholamzadehmir, C. Del Pero, S. Buffa, R. Fedrizzi, N. Aste, Adaptive-predictive control strategy for HVAC systems in smart buildings – a review, Sustain. Cities Soc. 63 (2020) 102480, https://doi.org/10.1016/j.scs.2020.102480.

[4] K. Rastogi, D. Lohani, Context-aware IoT-enabled framework to analyse and predict indoor air quality, Intell. Syst. Appl. 16 (2022) 200132, https://doi.org/10.1016/j.iswa.2022.200132.

[5] S. El Barrak, A. De La Garza, J. Mardis, T. Nguyen, M. Tran, J. Tzoc, A. Vallejo, P. Turner, D, Benhaddou, IoT-based smart airflow system for retrofitting commercial variable air volume HVAC systems, IFAC-PapersOnLine 55 (2022) 444–449. https://doi.org/10.1016/j.ifacol.2022.07.352.

[6] M.A. Abdulhussain, CFD pretending of vapor and liquid refrigerant mixing in variable speed scroll compressor, Eng. Sci. Technol. Int. J. 22 (2019) 168–176, https://doi.org/10.1016/j.jestch.2018.07.017.

[7] S. Ham, S. Choi, J.H. Jeong, Two-phase flow distribution in a refrigerant distributor having four indoor-unit connections of a variable refrigerant flow system, Int. J. Refrig. 126 (2021) 246–258, https://doi.org/10.1016/j.ijrefrig.2021.01.014.

[8] A.G. Devecioğlu, V. Oruç, Energetic performance analysis of R466A as an alternative to R410A in VRF systems, Eng. Sci. Technol. Int. J. 23 (2020) 1425–1433, https://doi.org/10.1016/j.jestch.2020.04.003.

[9] D. Kim, H. Cho, J. Koh, P. Im, Net-zero energy building design and life-cycle cost analysis with air-source variable refrigerant flow and distributed photovoltaic systems, Renew. Sustain. Energy Rev. 118 (2020) 109508, https://doi.org/10.1016/j.rser.2019.109508.

[10] H.C. Chuang, M.L. Guo, Z.H. Liao, C.T. Lee, Double-feedback control with stepless variable speed driving technology by sensing refrigerant pressure and indoor temperature applied to air conditioning system, Energy Build. 218 (2020) 110053, https://doi.org/10.1016/j.enbuild.2020.110053.

[11] B. Pandey, B. Bohara, R. Pungaliya, S.C. Patwardhan, R. Banerjee, A thermal comfort-driven model predictive controller for residential split air conditioner, J. Build. Eng. 42 (2021) 102513, https://doi.org/10.1016/j.jobe.2021.102513.

[12] C. Liu, T. Zhao, J. Zhang, T. Chen, X. Li, M. Xu, X. Yang, Operational electricity consumption analyze of VRF Air conditioning system and centralized air conditioning system based on building energy monitoring and management system, Procedia Eng. 121 (2015) 1856–1863, https://doi.org/10.1016/j.proeng.2015.09.167.

[13] J. Liu, J. Wang, G. Li, H. Chen, L. Shen, L. Xing, Evaluation of the energy performance of variable refrigerant flow systems using dynamic energy benchmarks based on data mining techniques, Appl. Energy 208 (2017) 522–539, https://doi.org/10.1016/j.apenergy.2017.09.116.

[14] Y. Guo, H. Chen, Fault diagnosis of VRF air-conditioning system based on improved Gaussian mixture model with PCA approach, Int. J. Refrig. 118 (2020) 1–11, https://doi.org/10.1016/j.ijrefrig.2020.06.009.

[15] Z. Zhou, G. Li, H. Chen, H. Zhong, Fault diagnosis method for building VRF system based on convolutional neural network: Considering system defrosting process and sensor fault coupling, Build. Environ. 195 (2021) 107775, https://doi.org/10.1016/j.buildenv.2021.107775.

[16] Y.P. Zhou, J.Y. Wu, R.Z. Wang, S. Shiochi, Energy simulation in the variable refrigerant flow air-conditioning system under cooling conditions, Energy Build 39 (2007) 212–220, https://doi.org/10.1016/j.enbuild.2006.06.005.

[17] R. Zhang, K. Sun, T. Hong, Y. Yura, R. Hinokuma, A novel variable refrigerant flow (VRF) heat recovery system model: Development and validation, Energy Build. 168 (2018) 399–412, https://doi.org/10.1016/j.enbuild.2018.03.028.

[18] G. Zhang, X. Li, W. Shi, B. Wang, Y. Cao, Influence of occupant behavior on the energy performance of variable refrigerant flow systems for office buildings: A case study, J. Build. Eng. 22 (2019) 327–334, https://doi.org/10.1016/j.jobe.2018.12.020.

[19] D. Kim, S.J. Cox, H. Cho, P. Im, Evaluation of energy savings potential of variable refrigerant flow (VRF) from variable air volume (VAV) in the U.S. climate locations, Energy Rep. 3 (2017) 85–93, https://doi.org/10.1016/j.egyr.2017.05.002.

[20] P.M. Ferreira, A.E. Ruano, S. Silva, E.Z.E. Conceição, Neural networks based predictive control for thermal comfort and energy savings in public buildings, Energy Build. 55 (2012) 238–251, https://doi.org/10.1016/j.enbuild.2012.08.002.

[21] A.E. Ruano, P.M. Ferreira, Neural network based HVAC predictive control, IFAC Proc. 47 (2014) 3617–3622, https://doi.org/10.3182/20140824-6-ZA-1003.01051.

[22] Y.Y. Ran, M.H. Jun, Performance based thermal comfort control (PTCC) using deep reinforcement learning for space cooling, Energy Build. 203 (2019) 109420, https://doi.org/10.1016/j.enbuild.2019.109420.

[23] L. Dong, Y. Li, J.M. House, T.I. Salsbury, Model-free control and staging for real-time energy efficient operation of a variable refrigerant flow system with multiple outdoor units, Appl. Therm. Eng. 180 (2020) 115787, https://doi.org/10.1016/j.applthermaleng.2020.115787.

[24] D. Woradechjumroen, H. Li, A. Deesiri, Development of coordination control for multiple rooftop units, Procedia Comput. Sci. 86 (2016) 176–179, https://doi.org/10.1016/j.procs.2016.05.050.

[25] D. Kim, J.E. Braun, J. Cai, D.L. Fugate, Development and experimental demonstration of a plug-and-play multiple RTU coordination control algorithm for small/medium commercial buildings, Energy Build. 107 (2015) 279–293, https://doi.org/10.1016/j.enbuild.2015.08.025.

[26] D. Woradechjumroen, H. Li, Y. Yu, Soft-repair technique for solving inherent oversizing effect on multiple rooftop units in commercial buildings, Build. Environ. 108 (2016) 47–62, https://doi.org/10.1016/j.buildenv.2016.08.020.

[27] A. Kobayashi, S. Shiochi, T. Suzuki, Y. Shimoda, Analysis of actual VRF system usage situation of urban university based on large amounts of operational data, in: Proceedings of the 18Th IBPSA Conference, 2023, pp. 3529–3536.